Bulgarian Journal of Physics vol. **XX** (20XX) 1–13

Projected Future Warming over Southeast Europe in the UNFCC Paris Agreement Context

H. Chervenkov*, **K. Slavov**
National Institute of Meteorology and Hydrology, Sofia 1784, Bulgaria
*Corresponding author Email: hristo.tchervenkov@meteo.bg

Received *6 December 2024*

Abstract. Today, there is a worldwide and substantial degree of agreement that the ongoing and projected future climate change, especially global warming, is the defining challenge of our time. Rising temperatures pose significant and far-reaching risks to human health, well-being, and other vulnerable systems. Climate change is a global emergency that goes beyond national borders and is an issue that requires international cooperation and coordinated solutions at all levels. The Paris Agreement is a legally binding international treaty on climate change, adopted by 196 Parties at the UN Climate Change Conference in Paris, France, on 12 December 2015. Its overarching goal is to hold "the increase in the global average temperature to well below 2°C above pre-industrial levels". Nowadays, much scientific research is dedicated to investigating future climatic changes and their spatial heterogeneity at 2°C warming. The eastern Mediterranean region, which includes Southeast Europe, is proving to be a 'hotspot' of climate change. The present study evaluates the projected future warming and the short-term thermal conditions over this region in the Paris Agreement context based on historical temperature data from the newest edition of the HadCRUT dataset and climate simulations from 25-member global circulation models' ensemble of the recently released NEX-GDDP CMIP6 product. The study provides strong evidence that the prescribed +2°C temperature threshold over Southeast Europe will be exceeded already in the coming decades, indicating also minor scenario dependence in near-term projections.

KEY WORDS: Climate Change, CMIP6, HadCRUT, NEX-GDDP, Southeast Europe, UNFCC Paris Agreement.

1 Introduction

Nowadays, there is a substantial degree of Agreement that the ongoing and projected future climate change is the defining challenge of our time. Rising temperatures pose significant risks to the ecosystem, biodiversity, and human health and

well-being. The degree of risk depends on various factors, including the intensity and duration of extreme heat events, as stated in the International Panel on Climate Change's (IPCC's) Summary for Policymakers [1]. In December 2015, the Paris Agreement [2] was approved by nearly 200 countries at the United Nations Framework Convention on Climate Change (UNFCC) 21st Conference of the Parties (COP 21). The Agreement's central aim is to strengthen the global response to the threat of climate change by keeping a global temperature rise below 2°C above pre-industrial levels this century and to pursue efforts to limit the temperature increase even further to 1.5°C. At the same time, the IPCC has accepted an invitation to prepare a special report on 1.5°C target in 2018 [3].

Previous studies regarding the 1.5°C and 2°C global warming levels have evidenced that land areas warm substantially faster than the oceans and high-latitude regions in the Northern Hemisphere show the fastest warming over the globe [4]. Research concerning these levels of global warming has also documented wide-ranging and far-reaching impacts on sectors including public health [5], water resources [6], and the economy [7]. The analysis in [8] of global mean temperature, precipitation, relative humidity, downwelling shortwave and longwave radiation, and wind speed over land under the high emission scenario reveals that the projected changes during the 2040s would be considerable. For a given increment in global mean temperature, the magnitude of temperature changes and the head-related events varies remarkably across regions [4, 9]. For example, the results in [10] show that the increases in mean temperature and temperature extremes over China are more significant than that in global mean temperature.

The eastern Mediterranean region, which includes Southeast Europe (SEE), is proving to be a 'hotspot' of climate change [11]. Alongside other findings, research has shown that projected summer warming is expected to exceed global rates by 40% [12].

Next to the global context, several studies are dedicated to the climate impacts in Europe under 1.5°C or 2°C global warming [13–15]. The results indicate that the world will likely pass the lower threshold in the coming decades. Cross-sectoral dimensions show the impacts of global warming that occur in parallel in more than one sector. As expected, impacts differ across industries and regions. For example, in [15], it is revealed that heat waves are already nearly twice as likely over southern Europe and the Mediterranean in a +1.5°C world. While most studies have highlighted global or synoptic-scale aspects of the projected changes at the 1.5°C and 2°C global warming levels, the relative share of publications considering the regional context is relatively tiny. According to our knowledge, none of them considers SEEu; thus, the present study could be considered novel.

General circulation models (GCMs) have been recognized as the primary tool for past and future climate simulations and impact assessments [8, 9, 13]. The

ongoing activities associated with the Coupled Model Intercomparison Project (CMIP) have demonstrated that a multi-model framework contributes to a more robust understanding of the Earth system and its processes. The models in CMIP6 generally have finer resolution with improved dynamic processes, and the new Shared Socioeconomic Pathway (SSP)-based scenarios are applied for simulations of the projected future climate [16, 17].

Based on these premises, this study uses CMIP6 data to determine the period when given regional warming threshold, +2°C, were crossed and, second, to assess the spatial distributions of the essential climate variables air temperature and precipitation sum as well as their long-term changes regarding the reference period.

After this introduction, Section 2 describes the study area and used data; The description of the applied methodology and the performed calculations is in Section 3; The core of the article is in Section 4 where the results are presented and discussed; The concluding remarks and the outlook for the further work are in Section 5.

2 Study Area and Used Data

The study area of SEEu has latitudinal and longitudinal boundaries of 35°N–50°N and 15° E–35°E, respectively, and is the same as in our previous works [18, 19]. In the latter one, it is described in detail, and its geographical map is also shown; therefore, for the sake of brevity, we will not describe it again now.

To define the +2°C period, we compare past observed and projected temperatures. The fact determines the selection of the pre-industrial period that it should not be affected by global warming in the 20th century [10], and thus we have chosen 1850–1900 as in the similar study [8]. We have sourced data from the observation-based data set HadCRUT, version 5.0.1.0 [20] covering a period of 1850–2021; hence, it is practically the single one covering the selected pre-industrial period. The HadCRUT is a global data set on a regular 5° latitude by 5° longitude grid with a temporal resolution of one month.

Due to our previous and very productive experience [18, 19] with the U.S. National Aeronautics and Space Administration (NASA) Earth eXchange Global Daily Downscaled Projections (NEX-GDDP) CMIP5 version, we have selected its successor, NEX-GDDP CMIP6 as source of GCM climate data for the near past and projected future. The NEX-GDDP-CMIP6 data sets contain bias-corrected and downscaled climate projections derived from the CMIP6 GCM simulations with four Tier 1 SSP scenarios: SSP1-2.6, SSP2-4.5, SSP3-7.0, and SSP5-8.5. These datasets provide a set of global, high-resolution in time (daily) and in space ($0.25^\circ \times 0.25^\circ$) seamless climate projection over land for the period from 1950 through 2014 (retrospective run) and from 2015 to 2100 (prospective run) by combining ground observations and native GCM results. It im-

proves CMIP6 simulations from large scale to regional-to-local scales with an unchanged long-term trend [21]. The publicly accessible NEX-GDDP temperature projections, with their high spatial resolution, allow us to perform assessments on finer scales, which is valued in the expert community [22–25].

The SSP scenario group Tier 1 consists of four 21st-century scenarios. Three of them, SSP1-2.6, SSP2-4.5, and SSP5-8.5, called 'Sustainability,' 'Middle of the Road,' and 'Fossil-fueled Development: Taking the Highway,' provide continuity with CMIP5 Representative Concentration Pathways (RCP) by targeting a similar level of aggregated radiative forcing [26]. With by 7 W·m^{-2} the year 2100, scenario SSP3-7.0 ('Regional Rivalry') is in the upper-middle part of the full range of scenarios. It was newly introduced after the RCP scenarios, closing the gap between RCP6.0 and RCP8.5.

3 Methodology and Performed Computations

The direct comparison of the multiyear mean temperatures for the past period and the projected future is hampered by two problems caused by the differences of both datasets, HadCRUT on the one hand and NEX-GDDP on the other:

- There is a nonnegligible disagreement between the spatial grids of both datasets.
- There is temporal inconsistency in the transition in time between the observation temperature data (HadCRUT) and modelled values (NEX-GDDP).

Hence, the HadCRUT grid has $5^\circ \times 5^\circ$ resolution, and the NEX-GDDP one with $0.25^\circ \times 0.25^\circ$ resolution, the first problem is obvious and requires that the HadCRUT data be aligned to the substantially finer NEX-GDDP grid. The procedure is not straightforward, and different approaches exist [27]. The proposed in [28] subgrid-scale mosaic scheme could be outlined due to its well-grounded physical basis and, at the same time, feasibility. In this scheme, each grid cell of the original 'coarse grid' is divided into N (in our case $N = 400$) regularly spaced subgrid cells of equal area, each with its topographical elevation (altitude) specification. For the temperature, the disaggregation is based on the difference between the topographical elevation of the coarse and corresponding fine grid cells. Preserving the original notation where the superscript sg refers to the subgrid and the overbar to the coarse grid, air temperature T at a subgrid cell i, j is obtained by

$$T_{i,j}^{sg} = \overline{T} + \Gamma_T \left(\overline{h} - h_{i,j}^{sg} \right), \tag{1}$$

where h denotes topographical elevation and Γ_T is an average tropospheric lapse rate of the temperature assumed to be equal to -6.5°C·km^{-1}. With the condition that

$$\overline{h} = \frac{1}{N} \sum_{i,j} h_{i,j}^{sg}, \tag{2}$$

we then have

$$\overline{T} = \frac{1}{N} \sum_{i,j} T_{i,j}^{sg} \tag{3}$$

so that temperature is conserved in the disaggregation process. Note that the coarse and subgrid-scale topography fields are constrained by Eq. 1.

The second problem is expressed in a step-wise transition in the data stream between the last year of HadCRUT (2014) and the first of NEX-GDDP (2015) and is due to the different nature of both datasets despite the embedded in the NEX-GDDP bias correction. It could be mitigated by applying additional bias correction using the observation-based data from HadCRUT, especially for the considered domain of SEE. Suitable solution in this regard is the described in [29] method of simple mean bias correction. Following the notations in this article, the simulated present-day model (predictor) time series of length N will be denoted as x_i^p, the corresponding observed (predictand) time series as y_i^p. The mean of the uncorrected model over a chosen present period μ_{raw}^p can be estimated as $\hat{\mu}_{raw}^p = \overline{x_i^p}$ (where the hat denotes the estimator, the overbar averaging in time as in Eq. 1–3), the corresponding real mean μ_{real}^p as $\hat{\mu}_{real}^p = \overline{y_i^p}$. An estimator of the model bias for present conditions is then given as

$$\widehat{Bias}\left(\mu^p\right) = \overline{x_i^p} - \overline{y_i^p}. \tag{4}$$

The simple mean bias correction method generates the future time series by subtracting the present-day model bias from the simulated future time series:

$$x_{i,corr}^f = x_{i,raw}^f - \widehat{Bias}\left(\mu^p\right) = x_{i,raw}^f - \left(\overline{x_{i,raw}^p} - \overline{y_i^p}\right). \tag{5}$$

Hence, HadCRUT provides the data in the form of monthly anomalies with respect to the multiyear means for 1961–1990 as well as the absolute values for this period; the first computation step is the calculation of the multiyear mean absolute values for 1850–1900 and 1950–2014, where the second one is needed for the bias correction. Next, we perform the spatial disaggregation, and the result is illustrated in Figure 1. Subsequently, we compute the bias for the near past conditions according to Eq. 4 using the dissagrageted HadCRUT data and NEX-GDDP data for the time frame 1950–2014; hence, this is the common overlapping period for historical data. Finally, we perform the bias correction of the NEX-GDDP future simulations according to Eq. 5. The last two steps are repeated for each of the selected 25 NEX-GDDP GCMs (see Table 1 in the Appendix for an explanatory list) and each scenario separately.

In the last decades, many researchers have favored a multimodel ensemble (MME) approach in which simulations are produced with multiple climate models due to the common understanding that the MME is usually superior to any individual model; hence, it effectively reduces random errors inherent in single models and dampens the influence of internal variability [25, 30]. As in our previous

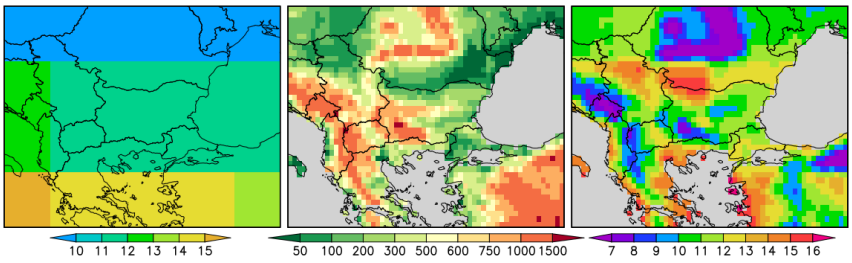

Figure 1. Spatial disaggregation of the multiyear mean temperature for 1850–1900: Original data in HadCRUT grid (left, unit: °C), Elevation data in NEX-GDDP grid (middle, unit: m) and disaggrgated temperature (right, unit: °C).

NEX-GDDP-based studies [18, 19], the MME approach is a crucial point of our evaluation concept. Thus, the MMEs median (MX50), 25th, and 75th percentile (lower and upper quartile, noted further MX25 and MX75) are calculated, and the estimations in the next section are based on these MME parameters.

All described computations are performed in a Linux environment, using Fortran programs and a wide variety of commands of the powerful tool cdo [31] incorporated in bash scripts.

4 Results and Discussion

4.1 Detection of the +2°C Crossing Year

The present study defines the +2°C crossing year similarly as in [8] namely as the time when the running 30-year mean regional near-surface air temperature reaches +2°C compared to the accepted pre-industrial period (1850–1900). The main differences to the latter study are two: i) regional, rather than global, temperature is considered, and ii) the assessment is performed for each grid cell separately rather than for the field mean temperature over the whole domain.

To obtain the +2°C crossing period, we compare the annual means of the past observed and projected future temperatures in terms of the MME MX25, MX50, and MX75 for each SSP. For the sake of brevity, however, the results for the marginal scenarios only, namely SSP1-2.6 and SSP5-8.5, are shown in Figures 2 and 3. As expected, the higher emission scenario (SSP5-8.5) in CMIP6 generally shows a faster temperature increase rate during the 21st century. Comparing the MME medians for both scenarios (second rows in Figures 2 and 3), it can be noticed that only a slight difference exists between the two SSPs in the 2040s, indicating minor scenario dependence in near-term projections. This outcome is also emphasized in [8] comparing the NEX-GDDP projections of the global near-surface temperature under SSP2-4.5 and SSP5-8.5. A specific spatial pattern of the warming dynamics can be hardly outdrawn except that the process

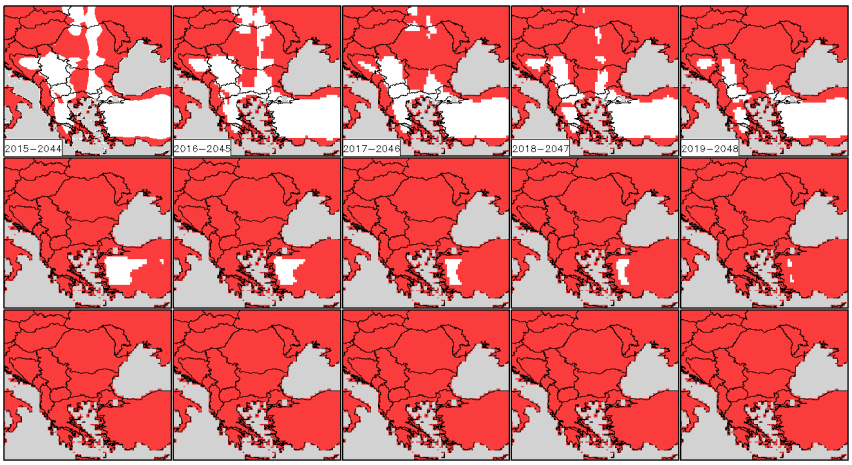

Figure 2. Spatial distribution of the the +2°C crossing year for MME MX25, MX50, and MX75 on the first, second and third row correspondingly for SSP1-2.6: The gridcells, where the running 30-year mean for the depicted period is greater than pre-industrial values are shown in red.

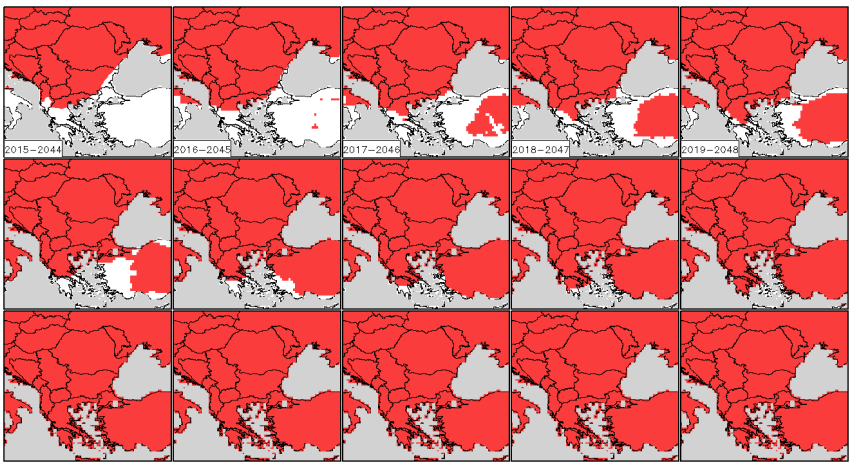

Figure 3. Same as Fig. 2 but for SSP5-8.5.

is slower over some parts of Asia Minor. The most significant result from the analysis of Figures 2 and 3 is, however, that for both scenarios, even for the first period, i.e., 2015–2044, the +2°C threshold is crossed over the prevailing part of the domain.

4.2 Short-term Change of the Mean Temperature

First, to demonstrate the MME spread for the near past climate conditions, Figure 4 shows the multiyear means for the 30-year period 1981-2010 MX25, MX50, and MX75.

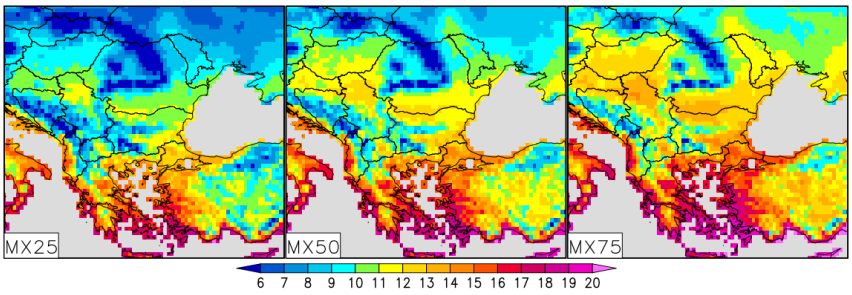

Figure 4. Multiyear means (unit: °C) for 1981–2010 of the MME's MX25, MX50 and MX75

The interquartile distance, i.e., the difference MX75-MX25, is below 2°C over the bigger part of the model domain, indicating the general absence of considerable differences between the models in this regard.

The short-term change of the mean temperature is estimated by comparing the multiyear mean of the MME's MX50 for the 30-year long period 2021— 2050 for each scenario with their equivalent for the near past shown in the middle subplot in Figure 4. The period 2021–2050 is selected; hence, according to

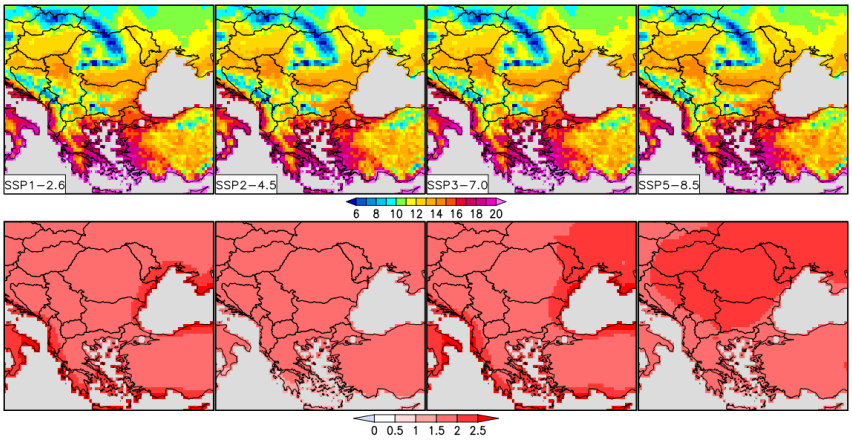

Figure 5. First row: Multiyear means (unit: °C) for 2021–2050 of the MME's MX50 for each scenario. Second row: absolute difference (unit: °C) between these parameters and their equivalent for 1981–2010.

Figures 2 and 3, the threshold of +2°C is crossed over the whole domain. The comparison is shown in Figure 5.

The same color legend is used to allow inter-comparison between Figure 4 and the first row of Figure 5. Figure 5 confirms the primary outcomes from subsection 4.1: It demonstrates, first of all, gradual increase of the magnitude of the warming from the low-emission scenario (SSP1-2.6) to the scenario with the strongest radiative forcing (SSP5-8.5). Nevertheless, at least for SSP1-2.6–SSP3-7.0, significant scenario dependence is absent. Finally, the projected short-term change of the mean temperature is everywhere positive without clear spatial distribution.

5 Conclusions

The study evaluates the projected warming over SEE in the context of the UNFCC Paris Agreement based on historical temperature data from HadCRUT and climate simulations from large GCM ensemble of the recently released NEX-GDDP CMIP6 product. The performed global scale thorough study [8] emphasizes the geographically varying patterns in the magnitude and direction of climate change and, subsequently, underlines the need for further work toward identifying regional specifics. The present investigation is a small step ahead in this direction.

Understanding future climate change and its spatial heterogeneity is critical to identifying where and to what extent human life and livelihoods will be at risk. This is a science-based premise for preparing policymakers for more effective plans to adapt and mitigate future climate change. The study shows unequivocally that over SEEu, the UNFCC-prescribed +2°C temperature threshold will be exceeded in the coming decades, and the differences between the emission scenarios are insignificant in general and in this respect.

Although the chosen methodology has limitations, replacing it with a more precise approach cannot change the general conclusions, which underlines the seriousness of the problem.

Acknowledgements

Hence this study is entirely based on freely available data and software, the authors would like to express their deep gratitude to the primary CMIP6 model output vendors as well as all other organizations and institutions (CCOLA, MPI-M, NASA), which provides free of charge software and data. Climate scenarios used were from the NEX-GDDP dataset, prepared by the Climate Analytics Group and NASA Ames Research Center using the NASA Earth Exchange, and distributed by the NASA Center for Climate Simulation (NCCS).

Appendix

Table 1. Descriptive list of the used 25 NEX-GDDP CMIP6 GCMs

No	Model name	Institution/country	Grid	Hor. Res. (lon.×lat.)
1	ACCESS-CM2	CSIRO-ARCCSS/Australia	192×144	1.875°×1.25°
2	ACCESS-ESM1-5	CSIRO/Australia	192×145	1.875°×1.25°
3	BCC-CSM2-MR	BCC/China	320×160	1.125°×1.125°
4	CanESM5	CCCma/Canada	128×64	2.813°×2.813°
5	CMCC-ESM2	CMCC/Italy	288×192	1.25°×0.94°
6	EC-Earth3	EC-Earth-Consortium/EC-Earth consortium	512×256	0.703°×0.703°
7	EC-Earth3-Veg-LR	EC-Earth-Consortium/EC-Earth consortium	512×256	0.703°×0.703°
8	FGOALS-g3	CAS/China	180×80	2°×2.025°
9	GFDL-ESM4	NOAA-GFDL/USA	288×180	1.25°×1°
10	INM-CM4-8	INM/Russia	180×120	2°×1.5°
11	INM-CM5-0	INM/Russia	180×120	2°×1.5°
12	IPSL-CM6A-LR	IPSL/France	144×143	2.5°×1.259°
13	KACE-1-0-G	NIMS-KMA/Republic of Korea	199×144	1.875°×1.25°
14	MIROC6	MIROC/Japan	256×128	1.403°×1.403°
15	MPI-ESM1-2-HR	MPI-M, DWD, DKRZ/Germany	384×192	0.939°×0.939°
16	MPI-ESM1-2-LR	MPI-M, AWI, DKRZ, DWD/Germany	192×96	1.875°×1.875°
17	MRI-ESM2-0	MRI/Japan	320×160	1.125°×1.125°
18	NorESM2-LM	NCC/Norway	144×96	2.5°×1.875°
19	NorESM2-MM	NCC/Norway	288×192	1.25°×0.94°
20	TaiESM1	AS-RCEC/Taiwan	288×192	1.25°×0.94°
21	CNRM-CM6-1	CNRM-CERFACS/France	128×64	2.813°×2.813°
22	CNRM-ESM2-1	CNRM-CERFACS/France	256×128	1.406°×1.406°
23	GISS-E2-1-G	NASA-GISS/USA	144×90	2.5°×2°
24	MIROC-ES2L	MIROC/Japan	256×128	1.406°×1.406°
25	UKESM1-0-LL	MOHC/UK	192×144	1.875°×1.25°

Bibliography

[1] IPCC (2023) Summary for Policymakers. In Climate Change 2023: Synthesis Report. Contribution of Working Groups I, II and III to the Sixth Assessment Report of the Intergovernmental Panel on Climate Change [Core Writing Team, H. Lee and J. Romero (eds.)]. IPCC, Geneva, Switzerland, 1-34, DOI: https://doi.org/10.59327/IPCC/AR6-9789291691647.001.

[2] United Nations Framework Convention on Climate Change (2015). Paris Agreement. Retrieved from http://unfccc.int/files/essential_background/ convention/application/pdf/english_paris_agreement.pdf.

[3] IPCC (2018) Summary for Policymakers. In Global Warming of 1.5 °C. An IPCC Special Report on the impacts of global warming of 1.5 °C above pre-industrial levels and related global greenhouse gas emission pathways, in the context of strengthening the global response to the threat of climate change, sustainable development, and efforts to eradicate poverty; Masson-Delmotte, V., Zhai, P.; Pörtner, H. O., Roberts, D., Skea, J., Shukla, P., Pirani, A., Moufouma-Okia, W., Péan, C., R. Pid-

cock, S. C., et al., (Eds.) Cambridge University Press: Cambridge, UK and New York, NY, USA, DOI: https://doi.org/10.1017/9781009157940.001.

[4] Seneviratne, S. I., Donat, M. G., Pitman, A. J., Knutti, R., Wilby, R. L. (2016) Allowable CO_2 emissions based on regional and impact-related climate targets. *Nature* **529**(7587), 477–483, Springer Science and Business Media LLC, DOI: https://doi.org/10.1038/nature16542.

[5] Ebi, K. L., Hasegawa, T., Hayes, K., Monaghan, A., Paz, S., Berry, P. (2018) Health risks of warming of 1.5°C, 2°C, and higher, above pre-industrial temperatures. *Env. Res. Lett.* **13**(6), 063007, IOP Publishing, DOI: https://doi.org/10.1088/1748-9326/aac4bd.

[6] Döll, P., Trautmann, T., Gerten, D., Schmied, H. M., Ostberg, S., Saaed, F., Schleussner, C.-F. (2018) Risks for the global freshwater system at 1.5°C and 2°C global warming. *Env. Res. Lett.* **13**(4), 044038, IOP Publishing, DOI: https://doi.org/10.1088/1748-9326/aab792.

[7] Pretis, F., Schwarz, M., Tang, K., Haustein, K., Allen, M. R. (2018) Uncertain impacts on economic growth when stabilizing global temperatures at 1.5°C or 2°C warming. *Philos. Trans. R. Soc. A* **376**(2119), 20160460, The Royal Society, DOI: https://doi.org/10.1098/rsta.2016.0460.

[8] Park, T., Hashimoto, H., Wang, W., Thrasher, B., Michaelis, A. R., Lee, T., Brosnan, I. G., Nemani, R. R. (2023) What Does Global Land Climate Look Like at 2°C Warming? *Earth's Fut.* **11**(5), American Geophysical Union (AGU), DOI: https://doi.org/10.1029/2022ef003330.

[9] Sillmann, J., Kharin, V. V., Zwiers, F. W., Zhang, X., Bronaugh, D. (2013) Climate extremes indices in the CMIP5 multimodel ensemble: Part 2. Future climate projections. *J. Geoph. Res.: Atmospheres* **118**(6), 2473–2493, American Geophysical Union (AGU), DOI: https://doi.org/10.1002/jgrd.50188.

[10] Shi, C., Jiang, Z.-H., Chen, W.-L., Li, L. (2018) Changes in temperature extremes over China under 1.5 °C and 2°C global warming targets. *Adv. Clim. Change Res.* **9**(2), 120–129, Elsevier BV. DOI: https://doi.org/10.1016/j.accre.2017.11.003.

[11] Lionello, P., Abrantes, F., Congedi, L., Dulac, F., Gacic, M., Gomis, D., Goodess, C., Hoff, H., Kutiel, H., Luterbacher, J., Planton, S., Reale, M., Schröder, K., Vittoria Struglia, M., Toreti, A., Tsimplis, M., Ulbrich, U., Xoplaki, E. (2012) Introduction: Mediterranean Climate—Background Information. *The Climate of the Mediterranean Region*, xxxv–xc, Elsevier, DOI: https://doi.org/10.1016/b978-0-12-416042-2.00012-4.

[12] Cramer, W., Guiot, J., Fader, M., Garrabou, J., Gattuso, J.-P., Iglesias, A., Lange, M. A., Lionello, P., Llasat, M. C., Paz, S., Peñuelas, J., Snoussi, M., Toreti, A., Tsimplis, M. N., Xoplaki, E. (2018) Climate change and interconnected risks to sustainable development in the Mediterranean. *Nat. Clim. Change* **8**(11), 972–980, Springer Science and Business Media LLC, DOI: https://doi.org/10.1038/s41558-018-0299-2.

[13] Vautard, R., Gobiet, A., Sobolowski, S., Kjellström, E., Stegehuis, A., Watkiss, P., Mendlik, T., Landgren, O., Nikulin, G., Teichmann, C., Jacob, D. (2014) The European climate under a 2°C global warming. *Env. Res. Lett.* **9**(3), 034006, IOP Publishing. DOI: https://doi.org/10.1088/1748-9326/9/3/034006.

[14] Arnell, N. W., Lowe, J. A., Lloyd-Hughes, B., Osborn, T. J. (2017) The impacts avoided with a 1.5°C climate target: a global and regional assessment.

Clim. Change **147**(1–2), 61–76, Springer Science and Business Media LLC. DOI: https://doi.org/10.1007/s10584-017-2115-9.

[15] Jacob, D., Kotova, L., Teichmann, C., Sobolowski, S. P., Vautard, R., Donnelly, C., Koutroulis, A. G., Grillakis, M. G., Tsanis, I. K., Damm, A., Sakalli, A., van Vliet, M. T. H. (2018) Climate Impacts in Europe Under +1.5° C Global Warming. *Earth's Future* **6**(2), 264–285, American Geophysical Union (AGU), DOI: https://doi.org/10.1002/2017ef000710.

[16] O'Neill, B. C., Tebaldi, C., van Vuuren, D. P., Eyring, V., Friedlingstein, P., Hurtt, G., Knutti, R., Kriegler, E., Lamarque, J.-F.; Lowe, J., et al. (2016) The Scenario Model Intercomparison Project (ScenarioMIP) for CMIP6. *Geosc. Model Dev.*, **9**, 3461–3482, DOI: https://doi.org/10.5194/gmd-9-3461-2016.

[17] Eyring, V., Bony, S., Meehl, G. A., Senior, C. A., Stevens, B., Stouffer, R. J., Taylor, K. E. (2016) Overview of the Coupled Model Intercomparison Project Phase 6 (CMIP6) experimental design and organization. *Geosc. Model Dev.* **9**(5) 1937–1958, Copernicus GmbH. DOI: https://doi.org/10.5194/gmd-9-1937-2016.

[18] Chervenkov, H., Slavov, K. (2022) NEX-GDDP Multimodel Ensemble vs. E-OBS — Evaluation of the Extreme Temperatures and Precipitation over Southeast Europe: Historical Comparison. *Atmosphere* **13**(4), p. 581, MDPI AG, DOI: https://doi.org/10.3390/atmos13040581.

[19] Chervenkov, H., Malcheva, K. (2023) Extreme Heat Events over Southeast Europe Based on NEX-GDDP Ensemble: Present Climate Evaluation and Future Projections. *Atmosphere* **14**(6), 1000, MDPI AG, DOI: https://doi.org/10.3390/atmos14061000.

[20] Morice, C. P., Kennedy, J. J., Rayner, N. A., Winn, J. P., Hogan, E., Killick, R. E., Dunn, R. J. H., Osborn, T. J., Jones, P. D., Simpson, I. R. (2021) An Updated Assessment of Near-Surface Temperature Change From 1850: The HadCRUT5 Data Set. *J. Geoph. Res.: Atmospheres*, **126**(3), American Geophysical Union (AGU), DOI: https://doi.org/10.1029/2019jd032361.

[21] Thrasher, B., Wang, W., Michaelis, A., Melton, F., Lee, T., Nemani, R. (2022) NASA Global Daily Downscaled Projections, CMIP6. *Sci. Data* **9**(1), Springer Science and Business Media LLC, DOI: https://doi.org/10.1038/s41597-022-01393-4.

[22] Jiang, F., Wen, S., Gao, M., Zhu, A. (2023) Assessment of NEX-GDDP-CMIP6 Downscale Data in Simulating Extreme Precipitation over the Huai River Basin. *Atmosphere*, **14**(10), 1497, MDPI AG, DOI: https://doi.org/10.3390/atmos14101497.

[23] Wu, F., Jiao, D., Yang, X., Cui, Z., Zhang, H., Wang, Y. (2023) Evaluation of NEX-GDDP-CMIP6 in simulation performance and drought capture utility over China — based on DISO. *Hydr. Res.*, **54**(5), 703–721, IWA Publishing, DOI: https://doi.org/10.2166/nh.2023.140.

[24] Gesangyangji, G., Holloway, T., Vimont, D. J., Acker, S. J. (2024) Future changes in state-level population-weighted degree days in the U.S. *Environ. Res. Lett.*, **19**,034029, IOP Publishing, DOI: https://doi.org/10.1088/1748-9326/ad28dd.

[25] Rao, K. K., Al Mandous, A., Al Ebri, M., Al Hameli, N., Rakib, M., Al Kaabi, S. (2024) Future changes in the precipitation regime over the Arabian Peninsula with special emphasis on UAE: insights from NEX-GDDP CMIP6 model simulations. *Sci. Rep.*, **14**(1), Springer Science and Business Media LLC,DOI: https://doi.org/10.1038/s41598-023-49910-8.

[26] Tebaldi, C., Debeire, K., Eyring, V., Fischer, E., Fyfe, J., Friedlingstein, P., Knutti, R., Lowe, J., O'Neill, B., Sanderson, B., van Vuuren, D., Riahi, K., Meinshausen, M., Nicholls, Z., Tokarska, K. B., Hurtt, G., Kriegler, E., Lamarque, J.-F., Meehl, G., et al. (2021) Climate model projections from the Scenario Model Intercomparison Project (ScenarioMIP) of CMIP6. *Earth Sys. Dyn.*, **12**(1), 253–293, Copernicus GmbH. DOI: https://doi.org/10.5194/esd-12-253-2021.

[27] Chervenkov H. (2016) Simple Postprocessing Method for Vertical Correction of Stratified Near-surface Atmospheric Parameters, *Bulg. Geoph. J.* **40**, 14–22.

[28] Giorgi, F., Francisco, R., Pal, J. (2003) Effects of a Subgrid-Scale Topography and Land Use Scheme on the Simulation of Surface Climate and Hydrology. Part I: Effects of Temperature and Water Vapor Disaggregation. *J. Hydromet.* **4**(2), 317–333, American Meteorological Society, DOI: https://doi.org/10.1175/1525-7541(2003)4<317:eoasta>2.0.co;2.

[29] Maraun, D. (2016) Bias Correcting Climate Change Simulations — a Critical Review. *Curr. Clim. Change Rep.*, **2**(4), 211–220, Springer Science and Business Media LLC, DOI: https://doi.org/10.1007/s40641-016-0050-x.

[30] Herger, N., Abramowitz, G., Knutti, R., Angélil, O., Lehmann, K., Sanderson, B. M. (2018) Selecting a climate model subset to optimise key ensemble properties. *Earth Sys. Dyn.* **9**(1), 135–151, Copernicus GmbH. DOI: https://doi.org/10.5194/esd-9-135-2018.

[31] Schulzweida, U. (2020) CDO User Guide. Available online: http://dx.doi.org/10.5281/zenodo.5614769 (accessed on 1 August 2024).